Yang Liu
Department of Engineering Mechanics,
School of Civil Engineering,
Shandong University,
Jinan 250061, China
e-mail: 1170569541@qq.com

Lingling Chen
Department of Engineering Mechanics,
School of Civil Engineering,
Shandong University,
Jinan 250061, China
e-mail: 2315689959@qq.com

Binglei Wang[1]
Department of Engineering Mechanics,
School of Civil Engineering,
Shandong University,
Jinan 250061, China
e-mail: bwang@sdu.edu.cn

Shengyou Yang
Department of Engineering Mechanics,
School of Civil Engineering,
Shandong University,
Jinan 250061, China;
Suzhou Research Institute,
Shandong University,
Jiangsu 215123, China
e-mail: 455950570@qq.com

Pradeep Sharma[1]
Department of Mechanical Engineering;
Department of Physics,
University of Houston,
Houston, TX 77204
e-mail: psharma@uh.edu

Tuning Crumpled Sheets for An Enhanced Flexoelectric Response

Flexoelectricity is a universal phenomenon present in all dielectrics that couples electrical polarization to strain gradients and vice-versa. Thus, structures and configurations that permit large strain gradients facilitate the design of an enhanced electromechanical coupling. In a recent work, we demonstrated the prospects for using crumpling of essentially arbitrary thin sheets for energy harvesting. Crumples, with their defect-like nature, admit singular and rapidly varying deformation fields and are thus ideal for engineering sharp non-uniformities in the strain field. In this work, we consider how to tune the design of crumpled sheets for a significant flexoelectric response. Specifically, we analytically derive the electromechanical coupling for a thin crumpled sheet with varying thickness and graded Young's modulus as key design variables. We show that the electromechanical coupling of such crumpled sheets can be tuned to be nearly five times those of the homogeneous film. [DOI: 10.1115/1.4052575]

1 Introduction

Crumpling an ordinary paper can produce electricity. This rather non-intuitive assertion was decisively addressed in a recent work [1]. The phenomenon that allows for this unexpected observation is flexoelectricity, a rather distinctive electromechanical coupling between polarization and strain gradients [2–6]. Since flexoelectricity exists in all dielectrics, as long as strongly inhomogeneous strains can be engineered, materials need not be piezoelectric to exhibit a non-trivial electromechanical coupling.

A notable aspect of flexoelectricity is the associated so-called size-effect [6,7]. As well appreciated in the mechanics literature, while in classical elasticity, strain fields (for a set of given boundary conditions) are invariant with respect to self-similar scaling, strain gradients increase dramatically with a reduction in feature size. Accordingly, for many materials, flexoelectricity acquires significant prominence only at characteristic length scales at the nanoscale. This has led to applications such as piezoelectric nanomaterials without using piezoelectric materials [8–11], nanoscale energy harvesting [12–16], sensors and actuators [17–20],

biological membranes [21–24], biophysical phenomena [25–27], defects [28,29], ferroelectric domain engineering, [30–33], flexoelectric semiconductors [34], soft matter [24,35,36], and many others.

The universal nature of flexoelectricity makes it an attractive avenue to engineer electromechanical coupling. Unfortunately, however, the flexoelectric coefficients of most materials are rather small. Researchers have pursued approaches to artificially enhance flexoelectricity by electret-like materials where charges and dipoles are embedded [16,37–40]. An alternative approach, which we pursue in this work, is to engineer large strain gradients. Heretofore, several strategies have been studied by researchers to produce large strain gradients, e.g., combining metallic nanowires with BST nanosheets [10], stacking thin sheets of disparate materials in certain order [8], and nano-sized triangular voids or inclusions in materials [41,42].

Germane to the topic of the current paper, flexoelectricity has also been investigated in the context of 2D materials including graphene [41,43–45] and biological membranes [21–24]. Indeed, elastic sheets or 2D material-like structure can easily bend and thus exhibit large changes in curvature (arguably the most facile way to induce inhomogeneous strains). Crumpling of flat sheets, a common occurrence in our daily lives as embodied with ordinary paper, can produce large curvatures. Recently, the mechanics of crumpling has attracted significant attention but has been mostly investigated purely as a mechanical and geometrical problem
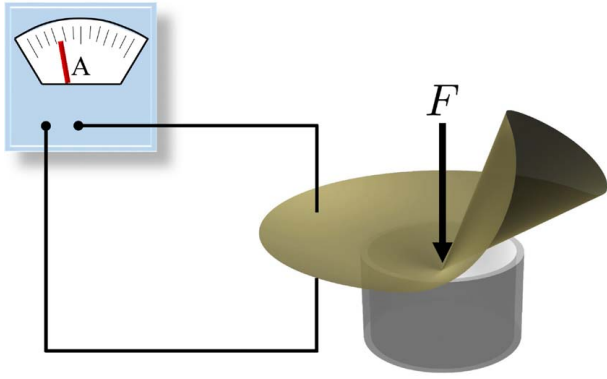
Fig. 1 Schematic of the generation of electricity from the crumpling of a thin dielectric film. The circular film is placed on a supporting structure (a hollow column in this picture) and a concentrated force is applied vertically to generate a crumpled sheet.

[46–50]. As shown in Fig. 1, a thin film is crumpled by a concentrated force which can induce large strain gradients near the deflection tip. In an interesting work, going beyond purely mechanical considerations, Kodali et al. [51] proposed the generation of electricity from the crumpling of polymer piezoelectric foils for potential applications in wearable electronics. Recently, Wang et al. recognized that due to flexoelectricity, crumpling of even an ordinary thin sheet ought to exhibit electromechanical coupling [1]. Specifically, we showed the emergence of a significant flexoelectric response due to large curvature at crumples, established scaling laws for the electromechanical behavior of crumpled flexoelectric thin sheets and showed that non-trivial energy harvesting may be achieved at submicron length scales.

While our prior work [1] established the usefulness of crumpling for flexoelectricity mediated energy harvesting, the question pertaining to how we might optimize or tune the electromechanical response remains unanswered. In this work, we propose the mechanics problem related to the crumpling of a flexoelectric thin sheet with varying elastic modulus and thickness. We are able to show, using both analytical means and simple numerical calculations, that variations of thickness and elastic modulus provide for an effective means to tune the flexoelectric response of a crumpled sheet and can be exploited for improving emergent electromechanical coupling. This paper is organized as follows. In Sec. 2, we present the theoretical formulation of the crumpling of thin sheets and the governing equations are obtained by using a variational approach. In Sec. 3, we discuss the electromechanical coupling for two illustrative cases: one is a circular sheet with varying thickness and the second is a circular sheet with graded Young's modulus. Conclusions are given in Sec. 4.

2 Theoretical Formulations

For a dielectric occupying a volume Ω bounded by a surface $\partial\Omega$, the total potential energy is given by [52]

$$U = \int_{\Omega} W^L(\nabla \boldsymbol{u}, \nabla\nabla \boldsymbol{u}, \boldsymbol{p}) - \frac{1}{2}\epsilon_0 |\nabla\xi|^2 + \boldsymbol{p} \cdot \nabla\xi \, dv$$
$$- \int_{\partial\Omega} Q\xi \, ds - \int_{\partial\Omega} \boldsymbol{t} \cdot \boldsymbol{u} \, ds \tag{1}$$

where ∇ is the gradient, $\boldsymbol{u}$ is the displacement, $\boldsymbol{p}$ is the polarization, ξ is the electric potential, Q is surface charge density, and $\boldsymbol{t}$ is the applied dead load, $\epsilon_0 = 8.85 \times 10^{-12}$ F/m is the vacuum permittivity, and $W^L(\nabla \boldsymbol{u}, \nabla\nabla \boldsymbol{u}, \boldsymbol{p})$ is the internal energy function.

Assuming independent variations of $\boldsymbol{u}$, $\boldsymbol{p}$, ξ and their gradients, the variation of the total potential energy δU is

$$\delta U = \int_{\Omega} \boldsymbol{T}\delta\nabla \boldsymbol{u} + \tilde{\boldsymbol{T}}\delta\nabla\nabla \boldsymbol{u} + \boldsymbol{E} \cdot \delta \boldsymbol{p}$$
$$- \epsilon_0 \nabla\xi \cdot \delta\nabla\xi + \nabla\xi \cdot \delta \boldsymbol{p} + \boldsymbol{p} \cdot \delta\nabla\xi \, dv$$
$$- \int_{\partial\Omega} Q\delta\xi \, ds - \int_{\partial\Omega} \boldsymbol{t} \cdot \delta \boldsymbol{u} \, ds \tag{2}$$

where

$$\boldsymbol{T} = \frac{\partial W^L}{\partial \nabla \boldsymbol{u}}, \quad \tilde{\boldsymbol{T}} = \frac{\partial W^L}{\partial \nabla\nabla \boldsymbol{u}}, \quad \boldsymbol{E} = \frac{\partial W^L}{\partial \boldsymbol{p}} \tag{3}$$

$\boldsymbol{T}$ is the second-order stress tensor, $\tilde{\boldsymbol{T}}$ is the third-order stress tensor, and $\boldsymbol{E}$ is the effective local electric field.

Hence, the first variation of the total potential energy (1) equals to zero at equilibrium and then gives

$$\nabla \cdot (\boldsymbol{T} - \nabla \cdot \tilde{\boldsymbol{T}}) = \boldsymbol{0} \quad \text{in } \Omega \tag{4}$$

$$\boldsymbol{E} + \nabla\xi = 0 \quad \text{in } \Omega \tag{5}$$

$$\nabla \cdot (-\epsilon_0 \nabla\xi + \boldsymbol{p}) = 0 \quad \text{in } \Omega \tag{6}$$

where the corresponding boundary conditions on $\partial\Omega$ are

$$(\boldsymbol{T} - \nabla \cdot \tilde{\boldsymbol{T}})\boldsymbol{n} - \hat{\nabla} \cdot (\tilde{\boldsymbol{T}}\boldsymbol{n}) = \boldsymbol{t} \quad \text{on } \partial\Omega \tag{7}$$

$$\tilde{\boldsymbol{T}}\boldsymbol{n} = 0 \quad \text{on } \partial\Omega \tag{8}$$

$$(-\epsilon_0 \nabla\xi + \boldsymbol{p}) \cdot \boldsymbol{n} = Q \quad \text{on } \partial\Omega \tag{9}$$

where $\hat{\nabla} \cdot (\tilde{\boldsymbol{T}}\boldsymbol{n}) = \nabla^{\parallel} \cdot (\tilde{\boldsymbol{T}}\boldsymbol{n}) - (\nabla^{\parallel} \cdot \boldsymbol{n})(\tilde{\boldsymbol{T}}\boldsymbol{n})\boldsymbol{n}$, $\nabla^{\parallel} = (\boldsymbol{I} - \boldsymbol{n} \otimes \boldsymbol{n})\nabla$ is the surface gradient operator [53] and $\boldsymbol{I}$ is the unit dyadic.

Within a linearized constitutive setting, the internal energy function $W^L(\nabla \boldsymbol{u}, \nabla\nabla \boldsymbol{u}, \boldsymbol{p})$ can be written as [54]

$$W^L = \frac{1}{2}\nabla \boldsymbol{u} \cdot \boldsymbol{c}\nabla \boldsymbol{u} + \frac{1}{2}\boldsymbol{p} \cdot \boldsymbol{a}\boldsymbol{p} + \boldsymbol{p} \cdot \boldsymbol{d}\nabla \boldsymbol{u} + \boldsymbol{p} \cdot \boldsymbol{f}\nabla\nabla \boldsymbol{u} + \frac{1}{2}\nabla\nabla \boldsymbol{u} \cdot \boldsymbol{g}\nabla\nabla \boldsymbol{u} \tag{10}$$

where the coefficients $\boldsymbol{c}$, $\boldsymbol{a}$, $\boldsymbol{d}$, $\boldsymbol{f}$, and $\boldsymbol{g}$ are material property tensors. The fourth-order tensor $\boldsymbol{c}$ is the elastic tensor. The second-order tensor $\boldsymbol{a}$ is the reciprocal dielectric susceptibility. The third-order tensor $\boldsymbol{d}$ is the piezoelectric tensor. The fourth-order tensor $\boldsymbol{f}$ is the flexoelectric tensor, and $\boldsymbol{g}$ is the sixth-order tensor related to the strain-gradient effect.

Finally, according to Eq. (3), the constitutive equations are

$$\boldsymbol{T} = \frac{\partial W^L}{\partial \nabla \boldsymbol{u}} = \boldsymbol{c}\nabla \boldsymbol{u} + \boldsymbol{d}\boldsymbol{p}$$

$$\tilde{\boldsymbol{T}} = \frac{\partial W^L}{\partial \nabla\nabla \boldsymbol{u}} = \boldsymbol{g}\nabla\nabla \boldsymbol{u} + \boldsymbol{f}\boldsymbol{p} \tag{11}$$

$$\boldsymbol{E} = \frac{\partial W^L}{\partial \boldsymbol{p}} = \boldsymbol{a}\boldsymbol{p} + \boldsymbol{d}\nabla \boldsymbol{u} + \boldsymbol{f}\nabla\nabla \boldsymbol{u}$$

2.1 Large Deflection of a Circular Film.
Consider a flat thin film of an isotropic dielectric materials (shown in Fig. 2). In terms of cylindrical polar coordinates (ρ, θ, z) with unit basis $(\boldsymbol{e}_\rho, \boldsymbol{e}_\theta, \boldsymbol{e}_z)$, the material point is denoted by $\boldsymbol{x} = \rho\boldsymbol{e}_\rho + z\boldsymbol{e}_z$ and the geometry of the film is defined in the reference region

$$0 \le \rho \le R_p, \quad 0 \le |\theta| \le \pi, \quad 0 \le z \le h \tag{12}$$

The upper surface of the circular film is at $z = 0$, the lower surface is at $z = h$ and the surrounding surface is at $\rho = R_p$. Typically, the middle surface of the film is at $z = h/2$.
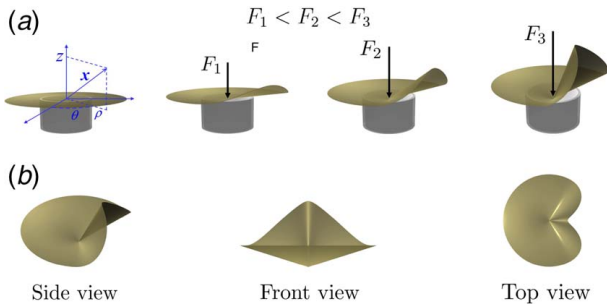
Fig. 2 Schematic of the crumpling of a circular film on a hollow column. (*a*) With the increase of a concentrated force *F*, the originally flat circular film gradually deforms to a crumpled film. A larger applied force corresponds to a deeper central deflection. (*b*) A crumpled circular film is observed in different directions

2.1.1 Displacement Vector. We first consider the deformation of the middle surface. With a mapping χ, a material point $\boldsymbol{x}$ on the middle surface is deformed to a spatial point $\boldsymbol{y} = \chi(\boldsymbol{x}) = \boldsymbol{x} + \boldsymbol{u}$, where $\boldsymbol{u}$ is the displacement vector. Note that the displacement vector on the middle surface is a function of two variables ρ and θ. We then decompose $\boldsymbol{u}$ into two parts: the in-plane displacement $\boldsymbol{u}_s$ and the out-of-plane deflection $\boldsymbol{u}_\perp$, i.e.,

$$\boldsymbol{u} = \boldsymbol{u}_s + \boldsymbol{u}_\perp \tag{13}$$

By the unit basis $(\boldsymbol{e}_\rho, \boldsymbol{e}_\theta, \boldsymbol{e}_z)$, we have

$$\boldsymbol{u}_s = u_\rho(\rho, \theta)\boldsymbol{e}_\rho + u_\theta(\rho, \theta)\boldsymbol{e}_\theta \quad \text{and} \quad \boldsymbol{u}_\perp = \zeta(\rho, \theta)\boldsymbol{e}_z \tag{14}$$

The flat film, as shown in Fig. 2, deforms into a developable cone (d-cone) shape when it is subjected to a vertically concentrated force. To model the d-cone phenomenologically, the d-cone can be approximately divided into two regions: the core region ($0 < \rho < R_c$) and the rest ($R_c < \rho < R_p$). Here, R_c is the core radius that denotes actually the region near the d-cone tip [49,50].

The out-of-plane deflection of crumples film can be assumed as follows:

$$\zeta(\rho, \theta) = \begin{cases} \zeta^*(\rho, \theta), & 0 < \rho < R_c \\ \alpha_1 \rho \psi^*(\theta), & R_c < \rho < R_p \end{cases} \tag{15}$$

As depicted in Fig. 2, α_1 is the ratio of the center deflection d to the supporter inner radius R and α_2 is the dimensionless core radius, i.e.,

$$\alpha_1 = \frac{d}{R} \quad \text{and} \quad \alpha_2 = \frac{R_c}{R} \tag{16}$$

Then, the dimensionless radius is $\hat{\rho} = \rho/R$. The deflection function $\zeta^*(\rho, \theta)$ in the core region is complicated, and its exact form is still an open problem. On the other hand, Cerda and Mahadevan [48] gave the form of the deflection function $\psi^*(\theta)$ away from the core region: $\psi^*(\theta) = H^*(|\theta| - \theta_1) + \tilde{\psi}(\theta)H^*(\theta_1 - |\theta|)$. Here, H^* is the Heaviside function and $\tilde{\psi}(\theta) = (\sin\theta_1 \cos\alpha\theta - \alpha\sin\alpha\theta_1 \cos\theta)/ (\sin\theta_1 \cos\alpha\theta_1 - \alpha\sin\alpha\theta_1 \cos\theta_1)$. As reported, $\alpha \approx 3.8$, $\theta_1 \approx 1.21$ rad, and the angle θ_1 is a material-independent constant and its magnitude is predicted to be $\theta_1 \approx 70°$ by Cerda and Mahadevan.

Moreover, the crumpled film in terms of the variation of the local curvature can be divided into two parts: the concave part ($-\theta_1 < \theta < \theta_1$) and the convex part ($\theta_1 < \theta < 2\pi - \theta_1$). As shown in Fig. 2, the applied force detaches the film from the supporting hoop in the concave part; however, the film still contacts the supporting hoop in the convex part.

2.1.2 Strain Tensor and Curvature Tensor. By the decomposed displacement vectors, the in-plane strain tensor $\boldsymbol{E}_s$ and the linearized curvature tensor $\boldsymbol{\kappa}$ can be defined as [55]

$$\boldsymbol{E}_s = \frac{1}{2}[\tilde{\nabla}\boldsymbol{u}_s + (\tilde{\nabla}\boldsymbol{u}_s)^T + \tilde{\nabla}\zeta \otimes \tilde{\nabla}\zeta] \tag{17}$$

$$\boldsymbol{\kappa} = -\tilde{\nabla}\tilde{\nabla}\zeta(\rho, \theta) \tag{18}$$

where the two-dimensional (in-plane) gradient operator $\tilde{\nabla}$ in cylindrical polar coordinates is $\tilde{\nabla} = \boldsymbol{e}_\rho\partial_\rho + \boldsymbol{e}_\theta\rho^{-1}\partial_\theta$. By Eqs. (14), (17), and (18), the in-plane strain tensor $\boldsymbol{E}_s$ and the curvature $\boldsymbol{\kappa}$ can be expressed in terms of functions u_ρ, u_θ, and ζ as

$$\boldsymbol{E}_s := \left[\partial_\rho u_\rho + \frac{1}{2}(\partial_\rho\zeta)^2\right]\boldsymbol{e}_\rho \otimes \boldsymbol{e}_\rho$$
$$+ \left[\frac{1}{2}\left(\frac{\partial_\theta u_\rho}{\rho} - \frac{u_\rho}{\rho} + \partial_\rho u_\theta + \frac{\partial_\rho\zeta\partial_\theta\zeta}{\rho}\right)\right]\boldsymbol{e}_\rho \otimes \boldsymbol{e}_\theta$$
$$+ \left[\frac{1}{2}\left(\frac{\partial_\theta u_\rho}{\rho} - \frac{u_\rho}{\rho} + \partial_\rho u_\theta + \frac{\partial_\rho\zeta\partial_\theta\zeta}{\rho}\right)\right]\boldsymbol{e}_\theta \otimes \boldsymbol{e}_\rho$$
$$+ \left[\frac{u_\rho}{\rho} + \frac{\partial_\theta u_\theta}{\rho} + \frac{1}{2}\frac{(\partial_\theta\zeta)^2}{\rho^2}\right]\boldsymbol{e}_\theta \otimes \boldsymbol{e}_\theta \tag{19}$$

and

$$\boldsymbol{\kappa} := [-\partial_{\rho\rho}\zeta]\boldsymbol{e}_\rho \otimes \boldsymbol{e}_\rho + \left[-\frac{\partial_{\rho\theta}\zeta}{\rho} + \frac{\partial_\theta\zeta}{\rho^2}\right]\boldsymbol{e}_\rho \otimes \boldsymbol{e}_\theta$$
$$+ \left[-\frac{\partial_{\rho\theta}\zeta}{\rho} + \frac{\partial_\theta\zeta}{\rho^2}\right]\boldsymbol{e}_\theta \otimes \boldsymbol{e}_\rho + \left[-\frac{\partial_\rho\zeta}{\rho} - \frac{\partial_{\theta\theta}\zeta}{\rho^2}\right]\boldsymbol{e}_\theta \otimes \boldsymbol{e}_\theta \tag{20}$$

In the outer region ($R_c < \rho < R_p$), the condition of inextensibility requires that the stretching strains vanish at moderate deflections [48]. By using the out-of-plane deflection $\zeta(\rho, \theta) = \alpha_1\rho\psi^*(\theta)$ in $R_c < \rho < R_p$, the in-plane strain tensor $\boldsymbol{E}_s$ and the linearized curvature tensor $\boldsymbol{\kappa}$ in Eqs. (19) and (20) are obtained as

$$\boldsymbol{E}_s = \boldsymbol{0}, \quad \boldsymbol{\kappa} := -\frac{\alpha_1}{\rho}[\partial_{\theta\theta}\psi^*(\theta) + \psi^*(\theta)]\boldsymbol{e}_\theta \otimes \boldsymbol{e}_\theta \tag{21}$$

In contrast, the curvature around the crumple tip is sufficiently large; therefore, we can only approximately determine the orders of the in-plane strain and curvature. As observed in experiments [49,50], the orders are $|\boldsymbol{E}_s| \sim (\alpha_1\alpha_2)^2$ and $|\boldsymbol{\kappa}| \sim \frac{\alpha_1}{\alpha_2}\frac{1}{R}$. Wang et al. [1] introduced two parameters $\lambda_E = 5.5$, $\lambda_\kappa = 5$ to amend these simplifications for small deformation. Hence, the magnitude of the strain tensor $\boldsymbol{E}_s$ and the curvature tensor $\boldsymbol{\kappa}$ are written as

$$|\boldsymbol{E}_s| \approx \lambda_E(\alpha_1\alpha_2)^2, \quad |\boldsymbol{\kappa}| \approx \lambda_\kappa\frac{\alpha_1}{\alpha_2}\frac{1}{R} \tag{22}$$

2.2 Maxwell's Equations and Electric Boundary Conditions. Since the film's thickness is much lower than its in-plane dimension, we mainly focus on the electric quantities in the thickness direction. The electric field is $e(z)$, the electric potential is $p(z)$, and the electric potential is $V(z)$.

From Maxwell's equations, the electric field is an irrotational field and

$$e(z) = -\frac{\partial V(z)}{\partial z} \tag{23}$$

Moreover, without free charges in the material, the Maxwell equation requires that

$$\frac{\partial[\epsilon_0 e(z) + p(z)]}{\partial z} = 0 \tag{24}$$

Integration with respect to z gives $\epsilon_0 e(z) + p(z) = \text{constant}$, $0 < z < h$. Next, we examine the electric boundary conditions. The electric

boundary conditions on the upper and lower surfaces are charge-controlled. In the absence of free charges, we have

$$\epsilon_0 e(z) + p(z) = 0, \quad \text{at } z = 0, h \tag{25}$$

Therefore, we have $e(z) = -p(z)/\epsilon_0$, $0 < z < h$.

We can further simplify the discussion by assuming constant electric and polarization field in the thickness direction. In other words, $e(z)$ and $p(z)$ and independent of z, and then the voltage difference between the upper and lower surfaces is

$$\Delta V = eh = -\frac{ph}{\epsilon_0} \tag{26}$$

2.3 Energy Formulation of Thin Films. For dielectric films, the internal energy function (per unit area of the neutral surface) can be written as [54]

$$W^L = \frac{1}{2}\left\{C_s|\boldsymbol{E}_s|^2 + C_b[tr(\boldsymbol{\kappa})]^2\right\} \\ + \frac{1}{2}\left\{a\,p^2 + 2pd_s tr(\boldsymbol{E}_s) + 2pf_s tr(\boldsymbol{\kappa}) + g[tr(\boldsymbol{\kappa})]^2\right\} \tag{27}$$

The first term on the RHS is the purely elastic energy, $C_s = ((1 - \nu^2)/12)Eh$ is the in-plane stiffness and $C_b = \frac{1}{12}Eh^3$ is the bending stiffness. The parameter $a = 1/(\epsilon - \epsilon_0)$ corresponds to the reciprocal dielectric susceptibility, ϵ is the material permittivity. d_s, f_s, and $g = El_0^2$ are parameters that are related to the piezoelectric, flexoelectric, and strain-gradient effects, respectively, and l_0 is the material length.

From the variation of the energy function (27), the electric field e is $e = \partial W^L/\partial p$. Combining the result $e = -p/\epsilon_0$ obtained in Sec. 2.3, we have

$$p = -[d_s tr(\boldsymbol{E}_s) + f_s tr(\boldsymbol{\kappa})]/(a + \epsilon_0^{-1}) \tag{28}$$

which directly shows that, in the case of nonpiezoelectricity $d_s = 0$, the polarization is proportional to the mean curvature $1/2 tr(\boldsymbol{\kappa})$. Such a linear relation has been reported in the biological context [5,39,56] and for crystalline membranes [44,45].

By substituting the linear relation into the energy function (27), the internal energy function W^L becomes a function of variables ρ and θ with two parameters α_1 and α_2. In addition, the potential work done by the centering dead load F is equal to $-Fd = -FR\alpha_1$. Collecting all the above expressions, we obtain the following final expression for the total energy in terms of α_1 and α_2:

$$U(\alpha_1, \alpha_2) = \frac{1}{2}\int_0^R\int_{-\pi}^{\pi}\left\{C_s|\boldsymbol{E}_s|^2 \right. \\ \left. + (K_s + K_s^*)[tr(\boldsymbol{\kappa})]^2\right\}\rho\,d\theta\,d\rho - FR\alpha_1 \tag{29}$$

where the coefficients $K_s = C_b + hg - hf_s^2/(a + \epsilon_0^{-1})$, $K_s^* = -hf_s^2(\eta^2 + 2\eta)/(a + \epsilon_0^{-1})$ with the ratio $\eta = d_s tr(\boldsymbol{E}_s)/[f_s tr(\boldsymbol{\kappa})]$. The first variation of the total potential energy (29) gives governing equations:

$$\frac{\partial U}{\partial \alpha_1}(\alpha_1, \alpha_2) = 0 \quad \text{and} \quad \frac{\partial U}{\partial \alpha_2}(\alpha_1, \alpha_2) = 0 \tag{30}$$

Solutions of the two algebraic equations (30) give the dimensionless center deflection α_1 and the core radius α_2. Thus, the curvature can be obtained by using Eqs. (21) and (22). After obtaining the curvature, the generated polarization p can be given by the relation Eq. (28). And, the induced charge is determined as $Q = \int_0^R\int_{-\pi}^{\pi}p\rho\,d\theta\,d\rho$.

2.3.1 Films With Varied Thickness. Supposing that the thickness of the film varies linearly along the radial direction of the film, that is,

$$h = h_0 + (n_1 - 1)\left(1 - \frac{\rho}{R_p}\right)h_0 \tag{31}$$

where h_0 is the thickness at the center of the film and n_1 is the ratio of the thickness at the center to the thickness at the outer, i.e., $n_1 = h(0)/h(R_p)$.

After some basic but tedious calculations, the non-dimensional energies of the core and the d-cone may be derived to be

$$\bar{U}_{core} = \frac{\frac{1}{2}\int_0^{R_c}\int_{-\pi}^{\pi}\left\{C_s|\boldsymbol{E}_s|^2 + (K_s + K_s^*)[tr(\boldsymbol{\kappa})]^2\right\}\rho\,d\theta\,d\rho}{\frac{1}{2}\pi R^2(C_b^0/h_0^2)} \\ = \alpha_1^4\alpha_2^6\bar{C}_s^0\lambda_E^2 + \frac{\bar{h}_0\alpha_1^2}{120\bar{R}_p^3}\left\{120\bar{h}_0\lambda_\kappa^2\bar{R}_p^3\left(\bar{K}_s^0 + \bar{K}_s^{*0}\right)\right. \\ + 15\alpha_2^2\bar{E}\bar{h}_0^2\lambda_\kappa^2\bar{R}_p n_1(n_1 - 1)^2 - 4\alpha_2^3\bar{E}\bar{h}_0^2\lambda_\kappa^2(n_1 - 1)^3 \\ - 20\alpha_2\bar{R}_p^2(n_1 - 1)\left[\bar{E}n_1^2\bar{h}_0^2\lambda_\kappa^2 + 4\bar{g}\bar{h}_0^2\lambda_\kappa^2 - 4\bar{h}_0\lambda_\kappa^2\bar{a}^*\bar{f}_s^2(\eta + 1)^2\right. \\ \left.\left. + \frac{1}{3}(1 - \nu^2)\alpha_1^2\alpha_2^6\bar{E}\lambda_E^2\right]\right\} \tag{32}$$

and

$$\bar{U}_{d-cone} = \frac{\frac{1}{2}\int_{R_c}^{R_d}\int_{-\pi}^{\pi}\left\{C_s|\boldsymbol{E}_s|^2 + (K_s + K_s^*)[tr(\boldsymbol{\kappa})]^2\right\}\rho\,d\theta\,d\rho}{\frac{1}{2}\pi R^2(C_b^0/h_0^2)} \\ = \frac{\bar{h}_0^2 I_1\alpha_1^2}{72\bar{R}_p^3}\left\{72\bar{a}^*\bar{f}_s^2\bar{R}_p^2(n_1 - 1)(\bar{R}_p - \alpha_2) + 72\bar{K}_s^0\bar{R}_p^3\ln\frac{\bar{R}_p}{\alpha_2}\right. \\ - \bar{h}_0(n_1 - 1)\left[9\bar{R}_p^3\bar{E}(n_1^2 + n_1) + 72\bar{R}_p^3\bar{g} - 18\alpha_2\bar{R}_p^2(\bar{E}n_1^2 + 4\bar{g})\right. \\ \left.\left. + 9\alpha_2^2\bar{E}\bar{R}_p(n_1^2 - n_1) + 2\bar{E}(n_1 - 1)^2\left(\bar{R}_p^3 - \alpha_2^3\right)\right]\right\} \tag{33}$$

where $I_1 = \int_{-1}^1[\partial_{\theta\theta}\psi^*(\pi\bar{\theta}) + \psi^*(\pi\bar{\theta})]^2 d\bar{\theta}$, $C_b^0 = Eh_0^3/12$, $a^* = 1/(a + \epsilon_0^{-1})$, and the dimensionless quantities are

$$\bar{h}_0 = \frac{h_0}{R}, \quad \bar{R}_p = \frac{R_p}{R}, \quad \bar{a}^* = \frac{a^*}{\epsilon_0}$$

$$\bar{C}_s^0 = C_s^0\Big/\frac{C_b^0}{h_0^2} = \frac{1 - \nu^2}{12}Eh_0\Big/\frac{C_b^0}{h_0^2}$$

$$\bar{K}_s^0 = K_s^0/C_b^0 = (C_b^0 + h_0g - h_0a^*f_s^2)/C_b^0$$

$$\bar{K}_s^{*0} = K_s^{*0}/C_b^0 = -h_0a^*f_s^2(\eta^2 + 2\eta)/C_b^0 \tag{34}$$

$$\bar{f}_s = f_s\Big/\sqrt{\frac{C_b^0}{h_0\epsilon_0}}, \quad \bar{E} = E\frac{Rh_0^2}{C_b^0}, \quad \bar{g} = g\frac{R}{C_b^0}$$

$$\bar{F} = FR\Big/\left(\frac{1}{2}\pi R^2\frac{C_b^0}{h_0^2}\right)$$

The dimensionless energy associated with the external force gives

$$\bar{U}_F = -FR\alpha_1\Big/\left(\frac{1}{2}\pi R^2\frac{C_b^0}{h_0^2}\right) = -\bar{F}\alpha_1 \tag{35}$$

Finally, the dimensionless total energy is

$$\bar{U} = \bar{U}_{core} + \bar{U}_{d-cone} + \bar{U}_F \tag{36}$$

The first variation of the total potential energy $\delta U[\boldsymbol{u}, \boldsymbol{p}, \xi] = 0$ now becomes $\delta \bar{U}[\alpha_1, \alpha_2] = 0$. Hence, the governing equations can be written as the following form:

$$\frac{\partial \bar{U}[\alpha_1, \alpha_2]}{\partial \alpha_1} = 0, \quad \frac{\partial \bar{U}[\alpha_1, \alpha_2]}{\partial \alpha_2} = 0 \tag{37}$$

2.3.2 Films With Graded Young's Modulus. Assuming that Young's modulus of the film varies linearly along the radial direction of the film, that is

$$E = E_0 + (n_2 - 1)\left(1 - \frac{\rho}{R_p}\right)E_0 \tag{38}$$

where E_0 is the Young's modulus at the edge of the film and n_2 is the ratio of the Young modulus at the center to the Young modulus at the outer, i.e., $n_2 = E(0)/E(R_p)$.

The non-dimensional energies of the core and the d-cone parts are

$$
\begin{aligned}
\bar{U}_{core} &= \frac{\frac{1}{2}\int_0^{R_c}\int_{-\pi}^{\pi}\left\{C_s|\boldsymbol{E}_s|^2 + (K_s + K_s^*)[\mathrm{tr}(\boldsymbol{\kappa})]^2\right\}\rho \, \mathrm{d}\theta \, \mathrm{d}\rho}{\frac{1}{2}\pi R^2 (C_b^0/h^2)} \\
&= \frac{\alpha_1^2 \alpha_2 \bar{E}_0 \bar{h}^3 (1-n_2)}{18\bar{R}_p}\left[\bar{h}^2\lambda_\kappa^2 + 12\bar{l}_0^2\lambda_\kappa^2 + \alpha_1^2\alpha_2^6\lambda_E^2(1-\nu^2)\right] \\
&\quad + \alpha_1^4\alpha_2^6\bar{C}_s^0\lambda_E^2 + \alpha_1^2\bar{h}^2\lambda_\kappa^2\left(\bar{K}_s^0 + \bar{K}_s^*\right)
\end{aligned} \tag{39}
$$

and

$$
\begin{aligned}
\bar{U}_{d-cone} &= \frac{\frac{1}{2}\int_{R_c}^{R_p}\int_{-\pi}^{\pi}\left\{C_s|\boldsymbol{E}_s|^2 + (K_s + K_s^*)[\mathrm{tr}(\boldsymbol{\kappa})]^2\right\}\rho \, \mathrm{d}\theta \, \mathrm{d}\rho}{\frac{1}{2}\pi R^2(C_b^0/h^2)} \\
&= \frac{\alpha_1^2\bar{h}^2 I_1}{12\bar{R}_p}\bar{E}_0(1-n_2)\left(\bar{h}^3 + 12\bar{h}\bar{l}_0^2\right)(\bar{R}_p - \alpha_2) \\
&\quad + \alpha_1^2\bar{h}^2 I_1 \bar{K}_s^0 \ln\frac{\bar{R}_p}{\alpha_2}
\end{aligned} \tag{40}
$$

where $\quad I_1 = \int_{-1}^{1}[\partial_{\theta\theta}\psi^*(\pi\bar{\theta}) + \psi^*(\pi\bar{\theta})]^2 \, \mathrm{d}\bar{\theta}, \quad C_b^0 = E_0 h^3/12,$ $g_0 = E_0 l_0^2,$ and the dimensionless quantities

$$\bar{h} = \frac{h}{R}, \quad \bar{R}_p = \frac{R_p}{R}, \quad \bar{l}_0 = \frac{l_0}{R}, \quad \bar{E}_0 = E_0 R^3/C_b$$

$$\bar{C}_s^0 = C_s^0/\frac{C_b^0}{h^2} = \frac{1-\nu^2}{12}E_0 h/\frac{C_b^0}{h^2}$$

$$\bar{K}_s^0 = K_s^0/C_b^0 = (C_b^0 + hg_0 - ha^*f_s^2)/C_b^0 \tag{41}$$

$$\bar{K}_s^* = K_s^*/C_b^0 = -ha^*f_s^2(\eta^2 + 2\eta)/C_b^0$$

$$\bar{F} = FR\left/\left(\frac{1}{2}\pi R^2\frac{C_b^0}{h^2}\right)\right.$$

The dimensionless energy associated with the external force is

$$\bar{U}_F = -FR\alpha_1\left/\left(\frac{1}{2}\pi R^2\frac{C_b^0}{h^2}\right)\right. = -\bar{F}\alpha_1 \tag{42}$$

Finally, the dimensionless total energy is

$$\bar{U} = \bar{U}_{core} + \bar{U}_{d-cone} + \bar{U}_F \tag{43}$$

Thus, the governing equations can be obtained as

$$\frac{\partial \bar{U}[\alpha_1, \alpha_2]}{\partial \alpha_1} = 0, \quad \frac{\partial \bar{U}[\alpha_1, \alpha_2]}{\partial \alpha_2} = 0 \tag{44}$$

3 Results and Discussions

With the theory in place, we now study the electromechanical coupling of dielectric films with graded thickness and Young's modulus. The parameters used in our numerical calculations are consistent with those in Ref. [1]. The flexoelectric constant is chosen as $f_s = -179$ Nm/C. The geometrical and material parameters of a *homogeneous* film are $R_p = 50$ mm, $h_0 = 52 \, \mu$m, $E_0 = 5$ Gpa, and $d_s = 5$ pC/N. The nonlocal elastic coefficient is taken to be the same as in Ref. [1], $g = 4.5 \times 10^{-6}$ N. The radius of the supporting hoop is $R = 12.5$ mm.

3.1 Circular Films With Varied Thickness. To investigate the effects of varying thickness on the electromechanical coupling, we simply assume a linear variation of the thickness along the radius:

$$h = h_0 + (n_1 - 1)\left(1 - \frac{\rho}{R_p}\right)h_0 \tag{45}$$

where h_0 is the thickness at the outer, i.e., $h(R_p) = h_0$, and n_1 is the ratio of the thickness at the center to the thickness at the outer, i.e., $n_1 = h(0)/h(R_p)$. For linearly varied thickness, we can control the ratio n_1. For $0 < n_1 < 1$, the center part is thinner than the outer part, see Fig. 3, and vice versa. The case of $n_1 = 1$ corresponds to a uniform film.

In Fig. 4, we show the variation of the normalized center deflection α_1 and the core radius α_2, defined in Eq. (16), with respect to the
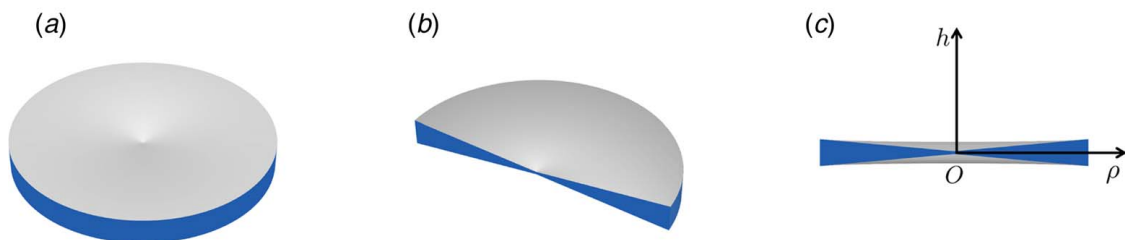

Fig. 3 (a) A circular film with varied thickness along the radius. The dielectric film is coated with two compliant electrodes on the top and bottom surfaces. (b) Semi-cut view of the circular film. (c) Coordinates are fixed on the semi-cut view.
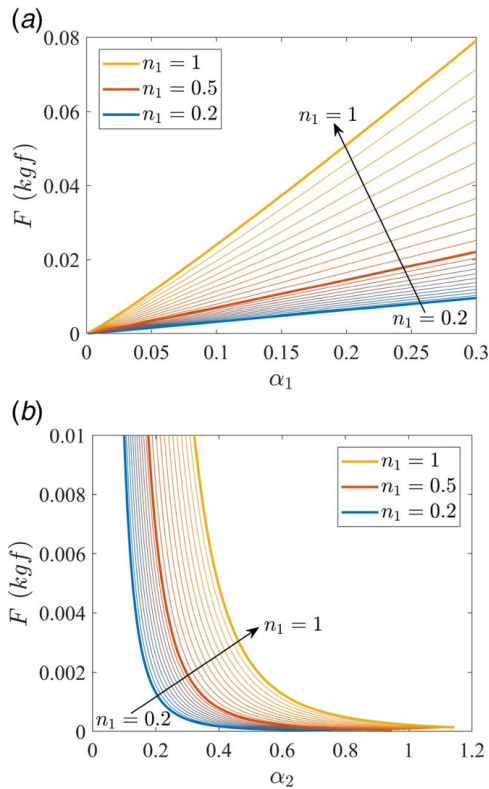
Fig. 5 The effective flexoelectric effect $\bar{d} = d^{eff}/d_0^{eff}$ versus non-dimensional scale factor γ for different films with varying thicknesses in Eq. (45)

Fig. 4 (a) Applied vertical force F versus dimensionless tip deflection α_1. (b) Applied vertical force F vs. dimensionless tip deflection α_2. Different ratio n_1 corresponds to different varied thickness in Eq. (45).

applied force F. For $n_1 = 1$ (uniform film), the deflection α_1 increases almost linearly with the increase of F while the core radius α_2 decreases nonlinearly with the increase of F. In this paper, we focus on small and modulate deflections, therefore, large deflection ($\alpha_1 > 0.3$) is excluded.

In Fig. 4(a), for a crumpled film at a given α_1, the smaller the ratio n_1, the smaller the applied force F. This is because a small tip deflection α_1 corresponds to a small bending stiffness and then a small applied force can induce a large deflection. Note that the deflection of thin films is almost proportional to the inverse of the bending stiffness, and bending stiffness is proportional to the cube of thickness. In other words, if the thickness of a homogeneous film is reduced by a half, the applied force is reduced to about 1/8 to achieve the same deflection. Such a phenomenon is also observed in Fig. 4(a).

In Fig. 4(b), for a given applied load, the smaller the ratio n_1, the smaller the core radius α_2. This interesting observation indicates that compared to a uniform film, a film with thinner thickness around the center has a smaller core size of the crumple. On the other hand, the thinner film has a much larger deflection than that of a homogeneous film at a given dead load. The two different
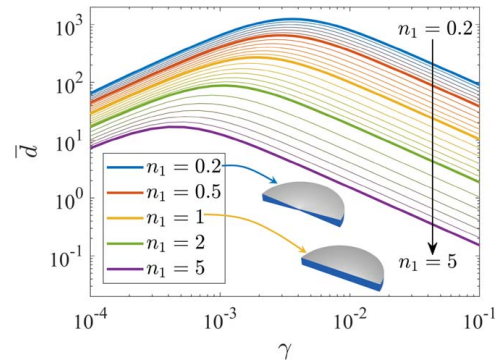
variations implies that there may exist a potential competition between deflection and crumpling.

One way to evaluate the intensity of electromechanical coupling is to determine the coefficient between induced charges Q and the applied force F, that is, $d^{eff} = Q/F$. The reference parameter is chosen to be $d_0^{eff} = 223$ pC/N. For homogeneous films with parameters $R_p = 50$ mm, $h_0 = 52$ μm, $E_0 = 5$ Gpa, and $d_s = 5$ pC/N, we investigate the coupling coefficient $d^{eff} = Q/F$ when the tip deflection at $\alpha_1 = d/R = 1/3$. Moreover, to study the size effects on the electromechanical coupling, we introduce a scale factor γ to control the dimensions, that is, $\gamma(R_p : R : h)$. Typically, $\gamma = 1$ and $n_1 = 1$ correspond to the originally uniform film.

In Fig. 5, the normalized coefficient $\bar{d} = d^{eff}/d_0^{eff}$ increases with the decrease of the film size (γ decreases from 1). The increase of the coefficient indicates that the electromechanical coupling noticeably depends on the structure size. However, the coefficient cannot increase monotonically with the decrease of the size. This is because that the purely elastic strain-gradient effects (mediated by the coefficient "g") plays an important role when the size decreases to nano scale. Here, we also focus on the effects of varying thicknesses (denoted by n_1) on the coupling.

The peak of the curve ($n_1 = 1$, a homogeneous film) in Fig. 5 is $\bar{d} = 270.4$ at $\gamma = 1.93 \times 10^{-3}$. However, the peak of the curve ($n_1 = 0.2$) is $\bar{d} = 1245.8$ at $\gamma = 3.63 \times 10^{-3}$. The comparison directly shows that a film with thinner thickness around the center can achieve a much higher electromechanical coupling, i.e., the center thickness decreases to 1/5 of the original thickness, the coupling coefficient approximately increases five times. Moreover, Fig. 5 demonstrates that, at the same scale factor γ for different dielectric films, a thinner film at the center corresponds to a larger coupling coefficient $\bar{d}$. Crumpling of dielectric films with graded thickness are able to generate increased flexoelectricity-mediated charge and thus have better electromechanical coupling performance.

3.2 Circular Films With Graded Young's Modulus. In contrast to films with graded thickness in the previous section, we now consider films with a linearly varying Young's modulus along the
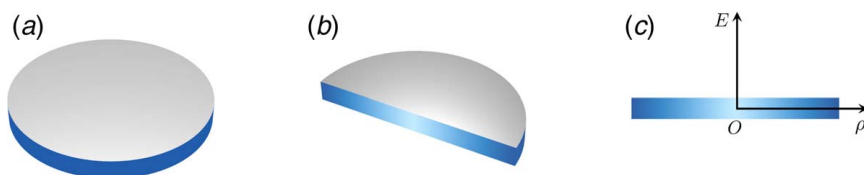

Fig. 6 (a) A circular film with graded Young's modulus along the radius. The dielectric film is coated with two compliant electrodes on the top and bottom surfaces. (b) Semi-cut view of the circular film. (c) Coordinates are fixed on the semi-cut view.
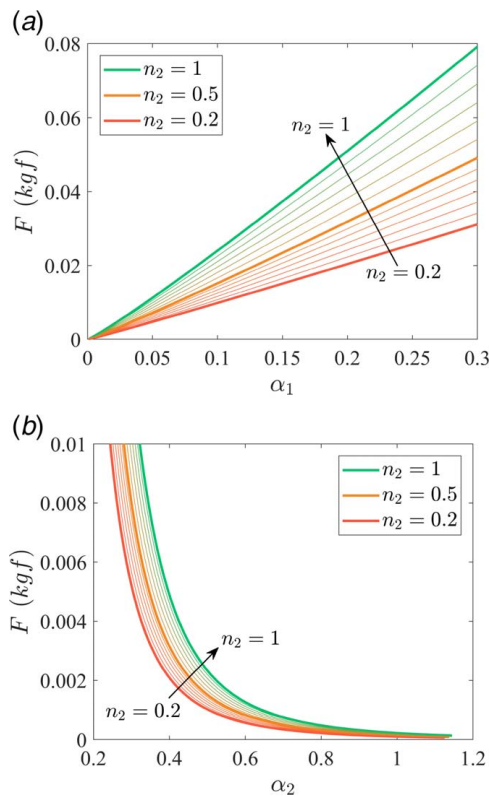
Fig. 7 (a) **Applied vertical force** F **versus dimensionless tip deflection** α_1. (b) **Applied vertical force** F **vs. dimensionless tip deflection** α_2. **Different ratio** n_2 **corresponds to different graded Young's modulus in Eq.** (46).

radius:

$$E = E_0 + (n_2 - 1)\left(1 - \frac{\rho}{R_p}\right)E_0 \qquad (46)$$

where E_0 is Young's modulus at the outer, i.e., $E(R_p) = E_0$, and n_2 is the ratio of the Young modulus at the center to that at the outer, i.e., $n_2 = E(0)/E(R_p)$. For $0 < n_2 < 1$, the center part is softer than the outer part, see Fig. 6, and vice versa. The case of $n_2 = 1$ denotes a homogeneous film.

In Fig. 7, we plot the variations of the normalized center deflection α_1 and the core radius α_2 with respect to the applied force F. With the increase of F, in the case of $n_2 = 1$, the deflection α_1 increases almost linearly but the core radius α_2 decreases nonlinearly. In Fig. 7(a) at a given α_1, a smaller ratio n_2 corresponds
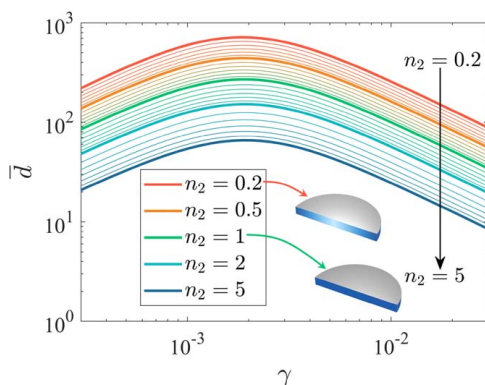

Fig. 8 **The effective flexoelectric effect** $\bar{d} = d^{eff}/d_0^{eff}$ **versus nondimensional scale factor** γ **for different films with graded Young's modulus in Eq.** (46)

to a smaller applied force F. This phenomenon is also observed in Fig. 4(a) since the bending stiffness is determined by both the Young modulus and thickness. The trends of curves in Fig. 7(b) are similar to those in Fig. 4(b), i.e., a smaller ratio n_2 corresponds to a smaller core radius α_2 for a given applied load, which indicates that a film with smaller Young's modulus around the center has a smaller core size of the crumple.

Similar to Fig. 5, we investigate the electromechanical coupling by scaling the dimensions of films in Fig. 8. We have discussed the size effect of the electromechanical coupling in Sec. 3.1. Here, we focus on the effects of graded Young's modulus (denoted by n_2) on the coupling. The peak of the curve ($n_2 = 1$) in Fig. 8 is $\bar{d} = 270.4$ at $\gamma = 1.93 \times 10^{-3}$. However, the peak of the curve ($n_2 = 0.2$) is $\bar{d} = 717.0$ at $\gamma = 1.93 \times 10^{-3}$. The comparison directly shows that a film with smaller Young's modulus around the center can achieve a much higher electromechanical coupling, i.e., the center Young's modulus decreases to 1/5 of the original Young's modulus, the coupling coefficient approximately increases 2.5 times. Moreover, we show that at the same scale factor γ for different dielectric films, a softer film at the center corresponds to a larger coupling coefficient $\bar{d}$. Like with the thickness, we conclude that gradation of Young's modulus in a flexoelectric crumpled sheet is an effective strategy to enhance electromechanical coupling.

4 Concluding Remarks

In the paper, we find that electromechanical coupling of crumpled 2D sheets can be tuned in a facile manner by varying the thickness and elastic properties of the underlying materials. Our results are largely analytical and hence can provide an easy guide for design. Gradation of thickness and elastic properties of 2D sheets is rather easily achievable by additive manufacturing based approaches. To tune electromechanical coupling, there exist optimum geometric sizes of the dielectric film with respect to certain geometric scale factors. For graded dielectric films, either thinning or softening films at the center can considerably improve the coupling compared to uniform homogeneous films.

Conflict of Interest

There are no conflicts of interest.

Data Availability Statement

The authors attest that all data for this study are included in the paper. No data, models, or codes were generated or used for this paper.

References

[1] Wang, B., Yang, S., and Sharma, P., 2019, "Flexoelectricity As a Universal Mechanism for Energy Harvesting From Crumpling of Thin Sheets," Phys. Rev. B, **100**(3), p. 035438.

[2] Tagantsev, A. K., 1986, "Piezoelectricity and Flexoelectricity in Crystalline Dielectrics," Phys. Rev. B Conden. Matter, **34**(8), p. 5883.

[3] Zubko, P., Catalan, G., and Tagantsev, A. K., 2013, "Flexoelectric Effect in Solids," Annu. Rev. Mater. Res., **43**, pp. 387–421.

[4] Mao, S., and Purohit, P. K., 2014, "Insights Into Flexoelectric Solids From Strain-Gradient Elasticity," J. Appl. Mech., **81**(8), p. 081004.

[5] Ahmadpoor, F., and Sharma, P., 2015, "Flexoelectricity in Two-Dimensional Crystalline and Biological Membranes," Nanoscale, **7**(40), pp. 16555–16570.

[6] Krichen, S., and Sharma, P., 2016, "Flexoelectricity: A Perspective on An Unusual Electromechanical Coupling," ASME J. Appl. Mech., **83**(3), p. 030801.

[7] Maranganti, R., Sharma, N., and Sharma, P., 2006, "Electromechanical Coupling in Nonpiezoelectric Materials Due to Nanoscale Nonlocal Size Effects: Green's Function Solutions and Embedded Inclusions," Phys. Rev. B, **74**(1), p. 014110.

[8] Sharma, N. D., Landis, C. M., and Sharma, P., 2010, "Piezoelectric Thin-Film Superlattices Without Using Piezoelectric Materials," J. Appl. Phys., **108**(2), p. 523.

[9] Fousek, J., Cross, L. E., and Litvin, D. B., 1999, "Possible Piezoelectric Composites Based on the Flexoelectric Effect," Mater. Lett., **39**(5), pp. 287–291.

[10] Chu, B., Zhu, W., Li, N., and Cross, L. E., 2009, "Flexure Mode Flexoelectric Piezoelectric Composites," J. Appl. Phys., **106**(10), p. 2069.

[11] Nguyen, T. D., Mao, S., Yeh, Y. W., Purohit, P. K., and Mcalpine, M. C., 2013, "Nanoscale Flexoelectricity," Adv. Mater., **25**(7), pp. 946–974.

[12] Majdoub, M. S., Sharma, P., and Çağin, T., 2009, "Dramatic Enhancement in Energy Harvesting for a Narrow Range of Dimensions in Piezoelectric Nanostructures," Phys. Rev. B, **78**(12), p. 121407(R).

[13] Jiang, X., Huang, W., and Zhang, S., 2013, "Flexoelectric Nano-Generator: Materials, Structures and Devices," Nano Energy, **2**(6), pp. 1079–1092.

[14] Deng, Q., Kammoun, M., Erturk, A., and Sharma, P., 2014, "Nanoscale Flexoelectric Energy Harvesting," Int. J. Solids. Struct., **51**(18), pp. 3218–3225.

[15] Choi, S. B., and Kim, G. W., 2017, "Measurement of Flexoelectric Response in Polyvinylidene Fluoride Films for Piezoelectric Vibration Energy Harvesters," J. Phys. D Appl. Phys., **50**(7), p. 075502.

[16] Rahmati, A. H., Yang, S., Bauer, S., and Sharma, P., 2019, "Nonlinear Bending Deformation of Soft Electrets and Prospects for Engineering Flexoelectricity and Transverse (d_{31}) Piezoelectricity," Soft. Matter., **15**(1), pp. 127–148.

[17] Wang, Z., Zhang, X. X., Wang, X., Yue, W., Li, J., Miao, J., and Zhu, W., 2013, "Giant Flexoelectric Polarization in a Micromachined Ferroelectric Diaphragm," Adv. Funct. Mater., **23**(1), pp. 124–132.

[18] Abdollahi, A., and Arias, I., 2015, "Constructive and Destructive Interplay Between Piezoelectricity and Flexoelectricity in Flexural Sensors and Actuators," ASME J. Appl. Mech., **82**(12), p. 121003.

[19] Bhaskar, U. K., Banerjee, N., Abdollahi, A., Solanas, E., Rijnders, G., and Catalan, G., 2016, "Flexoelectric Mems: Towards An Electromechanical Strain Diode," Nanoscale, **8**(3), pp. 1293–1298.

[20] Bhaskar, U. K., Banerjee, N., Abdollahi, A., Wang, Z., Schlom, D. G., Rijnders, G., and Catalan, G., 2016, "A Flexoelectric Microelectromechanical System on Silicon," Nat. Nanotechnol., **11**(3), pp. 263–266.

[21] Petrov, A. G., 2002, "Flexoelectricity of Model and Living Membranes," BBA – Biomembranes, **1561**(1), pp. 1–25.

[22] Petrov, A. G., 2006, "Electricity and Mechanics of Biomembrane Systems: Flexoelectricity in Living Membranes," Anal. Chim. Acta., **568**(1–2), pp. 70–83.

[23] Liu, L. P., and Sharma, P., 2013, "Flexoelectricity and Thermal Fluctuations of Lipid Bilayer Membranes: Renormalization of Flexoelectric, Dielectric, and Elastic Properties," Phys. Rev. E, **87**(3), pp. 1079–1094.

[24] Deng, Q., Liu, L., and Sharma, P., 2014, "Flexoelectricity in Soft Materials and Biological Membranes," J. Mech. Phys. Solids., **62**, pp. 209–227.

[25] Brownell, W. E., Spector, A. A., Raphael, R. M., and Popel, A. S., 2001, "Micro- and Nanomechanics of the Cochlear Outer Hair Cell," Annu. Rev. Biomed. Eng., **3**(1), pp. 169–194.

[26] Vasquez-Sancho, F., Abdollahi, A., Damjanovic, D., and Catalan, G., 2018, "Flexoelectricity in Bones," Adv. Mater., **30**(1705316), pp. 1–5.

[27] Deng, Q., Ahmadpoor, F., Brownell, W. E., and Sharma, P., 2019, "The Collusion of Flexoelectricity and Hopf Bifurcation in the Hearing Mechanism," J. Mech. Phys. Solids., **130**, pp. 245–261.

[28] Porenta, T., Ravnik, M., and Zumer, S., 2010, "Effect of Flexoelectricity and Order Electricity on Defect Cores in Nematic Droplets," Soft. Matter., **7**(1), pp. 132–136.

[29] Mao, S., and Purohit, P. K., 2015, "Defects in Flexoelectric Solids," J. Mech. Phys. Solids., **84**, pp. 95–115.

[30] Catalan, G., Lubk, A., Vlooswijk, A. H. G., Snoeck, E., Magen, C., Janssens, A., Rispens, G., Rijnders, G., Blank, D. H. A., and Noheda, B., 2011, "Flexoelectric Rotation of Polarization in Ferroelectric Thin Films," Nat. Mater., **10**(12), pp. 963–967.

[31] Glinchuk, M. D., Eliseev, E. A., and Morozovska, A. N., 2016, "Spontaneous Flexoelectric Effect in Nanosystems (topical Review)," Ferroelectrics, **500**(1), pp. 90–98.

[32] Cao, Y., Morozovska, A., and Kalinin, S. V., 2017, "Pressure-Induced Switching in Ferroelectrics: Phase-Field Modeling, Electrochemistry, Flexoelectric Effect, and Bulk Vacancy Dynamics," Phys. Rev. B, **96**(18), p. 184109.1.

[33] Mbarki, R., Baccam, N., Dayal, K., and Sharma, P., 2014, "Piezoelectricity Above the Curie Temperature? Combining Flexoelectricity and Functional Grading to Enable High-Temperature Electromechanical Coupling," Appl. Phys. Lett., **104**(12), p. 122904.

[34] Qu, Y., Jin, F., and Yang, J., 2020, "Effects of Mechanical Fields on Mobile Charges in a Composite Beam of Flexoelectric Dielectrics and Semiconductors," J. Appl. Phys., **127**(19), p. 194502.

[35] Codony, D., Gupta, P., Marco, O., and Arias, I., 2021, "Modeling Flexoelectricity in Soft Dielectrics At Finite Deformation," J. Mech. Phys. Solids., **146**, p. 104182.

[36] Grasinger, M., Mozaffari, K., and Sharma, P., 2021, "Flexoelectricity in Soft Elastomers and the Molecular Mechanisms Underpinning the Design and Emergence of Giant Flexoelectricity," Proc. Natl. Acad. Sci. U. S. A., **118**(21), p. e2102477118.

[37] Deng, Q., Liu, L., and Sharma, P., 2014, "Electrets in Soft Materials: Nonlinearity, Size Effects, and Giant Electromechanical Coupling," Phys. Rev. E, **90**(1), p. 012603.

[38] Wen, X., Li, D., Tan, K., Deng, Q., and Shen, S., 2019, "Flexoelectret: An Electret With a Tunable Flexoelectriclike Response," Phys. Rev. Lett., **122**(14), p. 148001.

[39] Ahmadpoor, F., Deng, Q., Liu, L. P., and Sharma, P., 2013, "Apparent Flexoelectricity in Lipid Bilayer Membranes Due to External Charge and Dipolar Distributions," Phys. Rev. E, **88**(5), p. 050701.

[40] Darbaniyan, F., Dayal, K., Liu, L., and Sharma, P., 2019, "Designing Soft Pyroelectric and Electrocaloric Materials Using Electrets," Soft. Matter., **15**(2), pp. 262–277.

[41] Chandratre, S., and Sharma, P., 2012, "Coaxing Graphene to Be Piezoelectric," Appl. Phys. Lett., **100**(2), p. 183.

[42] Sharma, P., 2004, "Size-Dependent Elastic Fields of Embedded Inclusions in Isotropic Chiral Solids," Int. J. Solids. Struct., **41**(22–23), pp. 6317–6333.

[43] Dumitric, T., Landis, C. M., and Yakobson, B. I., 2002, "Curvature-Induced Polarization in Carbon Nanoshells," Chem. Phys. Lett., **360**(1–2), pp. 182–188.

[44] Kalinin, S. V., and Meunier, V., 2008, "Electronic Flexoelectricity in Low-Dimensional Systems," Phys. Rev. B, **77**(3), p. 033403.

[45] Mohammadi, P., Liu, L., and Sharma, P., 2014, "A Theory of Flexoelectric Membranes and Effective Properties of Heterogeneous Membranes," J. Appl. Mech., **81**(1), p. 011007.

[46] Lobkovsky, A., Gentges, S., Li, H., Morse, D., and Witten, T. A., 1995, "Scaling Properties of Stretching Ridges in a Crumpled Elastic Sheet," Science, **270**(5241), pp. 1482–1485.

[47] Amar, M. B., and Pomeau, Y., 1997, "Crumpled Paper," Proc. R. Soc. A, **453**(1959), pp. 729–755.

[48] Cerda, E., and Mahadevan, L., 1998, "Conical Surfaces and Crescent Singularities in Crumpled Sheets," Phys. Rev. Lett., **80**(11), pp. 2358–2361.

[49] Cerda, E., Chaieb, S., Melo, F., and Mahadevan, L., 1999, "Conical Dislocations in Crumpling," Nature, **401**(6748), pp. 46–46.

[50] Cerda, E., and Mahadevan, L., 2005, "Confined Developable Elastic Surfaces: Cylinders, Cones and the Elastica," Proc. R. Soc. A Math. Phys. Eng. Sci., **461**(2055), pp. 671–700.

[51] Kodali, P., Saravanavel, G., and Sambandan, S., 2017, "Crumpling for Energy: Modeling Generated Power From the Crumpling of Polymer Piezoelectric Foils for Wearable Electronics," Flex. Print. Electron., **2**(3), p. 035005.

[52] Liu, L., 2013, "On Energy Formulations of Electrostatics for Continuum Media," J. Mech. Phys. Solids., **61**(4), pp. 968–990.

[53] Mindlin, R. D., 1964, "Micro-Structure in Linear Elasticity," Arch. Rational Mech. Anal., **16**(1), pp. 51–78.

[54] Sharma, N. D., Maranganti, R., and Sharma, P., 2007, "On the Possibility of Piezoelectric Nanocomposites Without Using Piezoelectric Materials," J. Mech. Phys. Solids., **55**(11), pp. 2328–2350.

[55] Landau, L. D., and Lifshitz, E. M., 1959, *Theory of Elasticity*, Pergamon Press, New York.

[56] Petrov, A. G., and Podgornik, R., 2000, "The Lyotropic State of Matter: Molecular Physics and Living Matter Physics," Phys. Today., **53**(9), pp. 67–68.